Title
Impacts of 2020 Beirut Explosion on Port Infrastructure and Nearby Buildings

Journal
Natural Hazards Review, 23(2)

ISSN
1527-6988

Authors
Sadek, Salah
Dabaghi, Mayssa
O'Donnell, Timothy M
et al.

Publication Date
2022-05-01

DOI
10.1061/(asce)nh.1527-6996.0000550

Impacts of 2020 Beirut Explosion on Port Infrastructure and Nearby Buildings

Salah Sadek[1], M. ASCE, Mayssa Dabaghi[1], A.M. ASCE, Timothy M. O'Donnell[2], S.M. ASCE, Paolo Zimmaro[2,3], M. ASCE, Youssef M.A. Hashash[4], F. ASCE, and Jonathan P. Stewart[2], F. ASCE

Abstract

At 18:08 on 4 August 2020, a large explosion occurred at Hangar 12 in the Port of Beirut. The size of the explosion was equivalent to that of an earthquake with local magnitude (M_L) of 3.3 (USGS). As one of the largest non-military explosions to ever impact an urban region, this event provides unprecedented opportunities to document explosion impacts on urban infrastructure. To facilitate this data collection, the Geotechnical Extreme Events Reconnaissance Association (GEER) coordinated a multi-agency response directed towards the collection of perishable data of engineering interest. Two main categories of infrastructure systems were impacted -- the Port of Beirut and the Beirut building stock. Within the Port, the explosion triggered a quay wall failure and flow slide, and strongly impacted grain silo structures that were in close proximity to Hangar 12. Within the city, a combination of historical masonry structures, older reinforced concrete structures, and modern high-rise structures was impacted. Through a combination of in-person inspections and street-view surveys, we collected data on structural performance (including damage to load-bearing elements) and building façades. Performance levels are classified according to procedures applied previously following earthquakes (for structural performance) and newly proposed procedures (for façade openings). We describe spatial distributions of these

[1] Maroun Semaan Faculty of Engineering and Architecture, American University of Beirut, Lebanon
[2] Civil & Environmental Engineering, University of California, Los Angeles (JPS: corresponding author)
[3] Environmental Engineering Department, University of Calabria, Italy
[4] Civil & Environmental Engineering, University of Illinois at Urbana-Champaign

damage types and dependencies on source distance and location-to-explosion direction. We demonstrate that physical damages are correlated to damage proxy maps produced by the Jet Propulsion Laboratory and the Earth Observatory of Singapore based on Copernicus Sentinel-1 satellite Synthetic Aperture Radar data, with a stronger correlation with structural damage than with façade damage.

Introduction

At 18:08 on 4 August 2020, a large explosion occurred at Hangar 12 in the Port of Beirut, Lebanon, at a facility storing Ammonium Nitrate. The death toll from the blast was at least 220, with injuries on the order of 7000. Hundreds of those injured were left with considerable and permanent scars and long term impairments. An estimated 300,000 people lost their homes and needed immediate temporary shelter. The direct damages to structures, infrastructure and other facilities were estimated at about 4 billion US$ with direct economic losses on the order of 3 billion US$ (World Bank Group, 2020).

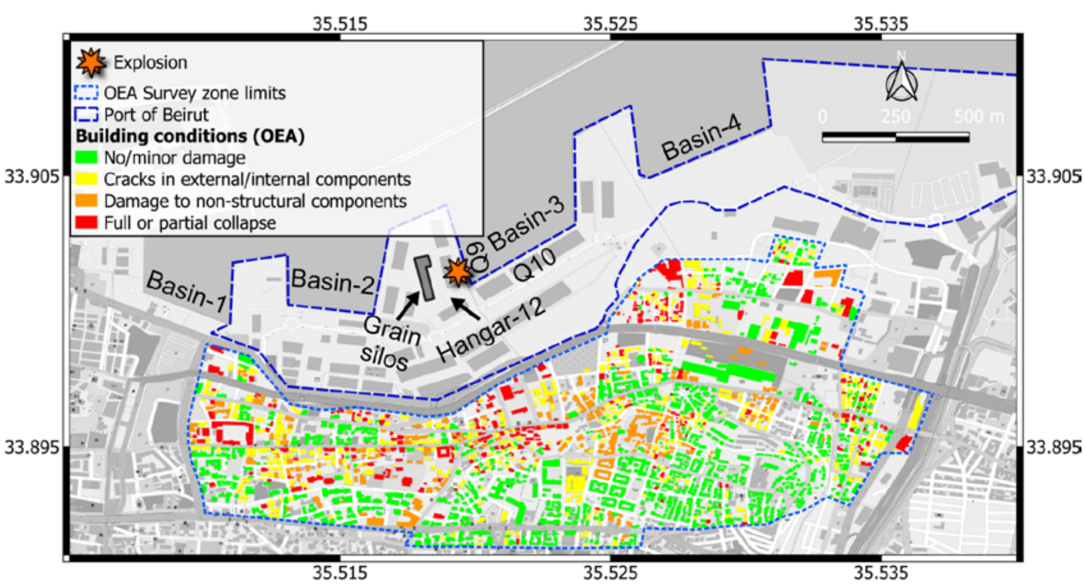

Figure 1: Map of Beirut showing the location of the explosion, Port of Beirut, and condition of the buildings surveyed by the Order of Engineers and Architects (OEA, 2020). Within the Port of Beirut, basin and quay wall numbers are provided.

A number of technical topics have been investigated in connection with this event, including the blast yield (around 0.50 kt TNT -- Rigby et al. 2020; Diaz 2020; Aouad et al. 2020; Pilger et al., 2020), generated seismic waves (Nemer, 2021), simulations of air pressure (blast) waves (Valsamos et al., 2021; Zhang et al. 2021), structural response of the Beirut silos (Temsah et al., 2021; Ismail et al., 2021), trauma experienced by people impacted by the blast (Al-Hajj et al. 2021), and risk/consequence analyses of the event (Yu et al. 2021). Whereas the Beirut event presents a number of unique features related to scope and context, the nature of the blast and its magnitude are comparable to the Toulouse AZF plant explosion of 2001 (Dechy et al., 2001).

In this article, we describe the impacts of the blast on physical infrastructure, based on reconnaissance coordinated by the Geotechnical Extreme Events Reconnaissance (GEER) association in collaboration with multiple governmental and university agencies in Beirut. In addition to present effort, a number of local and international agencies conducted immediate relief and assessment work (Beirut Order of Engineers and Architects, OEA 2020; Lebanese Red Cross 2020; Dar Group, 2020; Search and Rescue Assistance in Disasters, SARAID, 2020). In this paper, we focus on two main effects of the event:

1. The near-field impact of the explosion on Port of Beirut infrastructure, including apparent foundation deformations of the grain silos and failure of a quay wall with flow failure of retained artificial fill.
2. The spatially variable impacts of the explosion on buildings in Beirut. We document distributions of structural damage (i.e., affecting load-bearing elements) and exterior (façade) damage to building openings such as windows and doors.

Subsequent sections describe the information sources and data collection, the explosion impacts in the Port of Beirut, and the explosion impacts on buildings in Beirut. The paper is concluded with a summary and description of how the information compiled in this work can be useful in future research. An earlier version of the work presented here was presented in a GEER report (Sadek et al. 2021a). All data collected as part of this study is available on DesignSafe (Rathje et al., 2017) as a published dataset (Sadek et al., 2021b).

Information Sources and Data Collection

GIS Database

We utilize a Geographic Information System (GIS) database for Beirut created by the American University of Beirut Urban Lab (AUB-UL). The database includes cadastral information, buildings, roads, population and other-related data. For buildings, the AUB-UL GIS map includes location, approximate size, and date of construction. This information was derived from public sources, such as cadastral and assessor files at the finance ministry. Buildings in the AUB-UL inventory are shown in Figure 1 (color code is based on OEA surveys described further below).

Open Map Lebanon is a community-based endeavor formed after the August 4 blast to promote data dissemination and relief efforts. One of the tasks undertaken by Open Map Lebanon is street-level imagery, which is compiled using Mapillary. A large fraction of the images available on the Open Map Lebanon Mapillary application were contributed by Sadek et al. (2021b).

Order of Engineers and Architects (OEA) Surveys

On August 12, 2020, the Beirut Order of Engineers and Architects launched a large-scale field survey in the areas closest to and most affected by the blast, as illustrated in Figure 1. This effort was led by the OEA Public Safety Committee and utilized approximately one thousand volunteers of various specialties. A total of 3040 properties containing 2509 buildings were inspected in the designated area. The OEA generated weekly structural damage summary reports and a final report (OEA, 2020) and established a central data bank in which collected images and team reports were filed. Full access to this data remains pending.

The OEA documented the condition of the buildings they surveyed and provided building-specific recommendations of evacuation, closure, or strengthening (full or partial, immediately or during repair works) to the most damaged buildings. As shown in Figure 1, the damage was classified as follows: no damage, cracks in building components, damage to non-structural components, and risk of full/partial collapse. Relative to the blast site, the OEA inspections occurred up to 1 km west, 1 km south, and 1.5 km east, in the districts of Minet El-Hosn, Zokak El Blat, Port, Saifi, Rmeil, and Medawar. At the southern limit of the inspection areas, damage levels of “no/minor damage” were recorded, whereas appreciable damage was observed at the western and eastern margins of the surveyed area, suggesting that damage locations may extend beyond the limits of the OEA surveys. The OEA damage assessments shown in Figure 1 were obtained from their report (OEA 2020). Data from the most heavily damaged buildings inspected by the OEA was incorporated in the present study, as described in more detail in the section on Building Impacts.

Dar Group Surveys

The Dar Group is an engineering consulting firm based in Beirut. On behalf of the Beirut municipality, Dar Group performed street surveys of about 7000 buildings over the time interval August 11 to September 10, 2020 for the Beirut Municipality (Dar Group, 2020). These surveys consisted of evaluating and photographing buildings from the street level (structures were generally not entered). The objective was to evaluate the extent of structural damage sustained by buildings (no damage, partial collapse or total collapse) in order to classify them as safe (green), restricted use (yellow) or unsafe (red) for occupants after the explosion. The investigation also included an assessment of the extent of façade damages in terms of estimated quantities of damaged glazing and cladding.

The Dar Group surveys covered a wider geographic extent compared to those of the OEA and included buildings in the districts of the Port, Achrafieh, Rmeil, Medawar, Mousseitbeh, Mazraa, Ain Mreisseh and Ras Beirut. Field reports along with images of the surveyed properties were obtained from Dar and integrated into the central database at the Beirut Urban Lab. This data was analyzed in reference to identifiable damage categories. It was not incorporated in the present study because the definitions of the structural damage categories used by DAR differ from the ones used in this study, and thus require further investigation for consistent damage classification. The facade damage data collected by DAR could also be incorporated in future studies.

<u>Lebanese Red Cross (LRC)</u>

In addition to the treatment and transport of the wounded and providing help in the evacuation of the damaged hospitals, the Lebanese Red Cross (LRC) also performed about 50,000 door-to-door household needs assessments, and provided direct cash assistance to about 10,000 vulnerable affected families for basic needs and urgent repairs. The LRC assessments included a shelter condition assessment that consisted of observations of structural damage and of damage to windows and external doors (LRC, 2020). Access to this data remains pending.

GEER Association Reconnaissance

The GEER association formed a reconnaissance team in August 2020 to examine the engineering impacts of the explosion with the aim of collecting and documenting perishable data. The emphasis of data collection was on impacts in the Port and in the city building stock, as noted in the *Introduction*. The data collection involved in-person reconnaissance and street view surveys, as described further below. In addition, we have incorporated data from other studies for the interpretation of structural damage patterns, namely OEA (2020).

Port Infrastructure Impacts

Port Facility

Beirut is one of the oldest cities in the world, continuously inhabited for more than 5,000 years. The city coastline and safe water harbor/port(s) have shifted westwards and northwards over various periods of expansion and reclamation. The earlier Phoenician port and associated dry docks were identified in recent archeological exploration as being well within the current center of the Beirut central district (approximately 300 m south of the current coastline). The Port of Beirut has seen periods of expansion and functionality change over the various eras. During the Roman presence (64 BC to the middle of the 6th century AD), it was developed into a commercial and economic center serving the “colonies”. This was followed by a succession of periods (Omayyad, Crusaders and Mameluke) in which the Port was the berth of armed fleets and later served as a hub for pilgrims visiting the holy lands.

The “modern” incarnation of the Beirut Port leading to its present extent started in the late 19th century when a concession was given by the Ottoman authorities to a private company to expand and manage the facility. Following World War I, under the French Mandate for Syria and Lebanon (i.e., a period of French oversight of local governance), the Port management company was reorganized and granted a new concession in 1925 that ended in 1960. From 1960 to 1990 a Lebanese company operated the Port, after which it was returned to the state. Figure 2 shows the significant expansions of the Port facilities that were made since 1875, including the number and size of docks, deeper drafts, and larger commercial and storage areas.

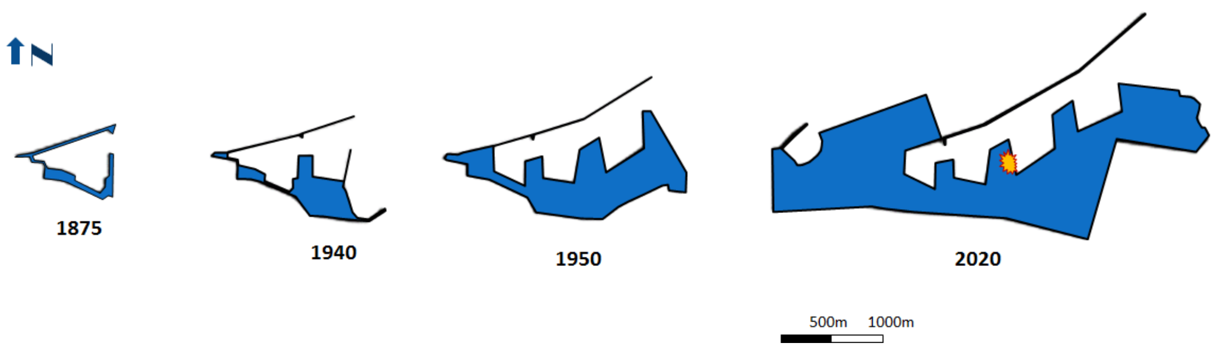

Figure 2: Scaled representation of Beirut Port expansion from 1875 to 2020. Explosion location marked in 2020 map.

In the past 30 years, further and more significant expansions of the Port were completed. These allowed for a large container facility and larger and deeper water docks, allowing the facility to receive the largest container/cargo vessels. As of 2019 the Beirut Port accounted for more than 60% of Lebanon's total imports (NY times, 2020) valued at roughly 25% of GDP. Figure 1 shows a map of the Port facility with its various basins and quays as it was before 4 August 2020.

Given the original footprint and sequence of expansion of the Port over time, the methods of construction and associated complexities were multiple and varied. In its earliest version(s) the Port was located in a natural "deep" water bay along a rocky portion of the shoreline. The earliest protective seawalls were built by dumping rock sourced from limestone quarries in the foothills closest to the shore. More modern expansions up to the 1950s (Figure 1: Basins 2 and 3) relied on concrete blocks to form quay walls with miscellaneous backfill to form the docks behind the newly established quays. As the Port expanded further east, particularly for Basin 4 and the newest deepwater quays facing north, large diameter driven piles were used to form the foundation of the walls and dock slabs, particularly in the zone of operation of the container cranes and handling equipment. The use of such foundation solutions was accompanied by ground improvement in the general dock areas in the container terminal. These consisted of preloading with wick drains placed in the seabed sediments in some locations along with complementary dynamic compaction of the granular fill.

In the mid to late 1960s plans were drawn and executed to build the largest grain storage facilities of their kind in the region. Phase I of the project consisted of 8 silo columns 3 rows deep. Phase II extended the facility to 14 silo columns 3 rows deep with a total capacity of 105,000 tons of grain, and was completed in 1969 (Figure 3). The Beirut Port Silos were considered a feat of engineering at the time. As shown in Figure 4, they consisted of 3 parallel rows of 14 cylindrical concrete silos, supported on 2900 driven precast reinforced concrete piles 12-15 m deep. Phase III saw the addition of 6 cells raising the total number of columns to 16 and the capacity to 150,000 tons. Figure 5 shows a soil profile at the site based on data from boreholes executed at the time of the planning for Phase-1 and provided by Forex sarl (a local site exploration company). Overburden-corrected Standard Penetration Test (SPT) data is shown for the approximately 13 m deep fill layer at this location. The average value of N_1 = 20 blow/ft; the energy level is unknown but is estimated as 45-60%.

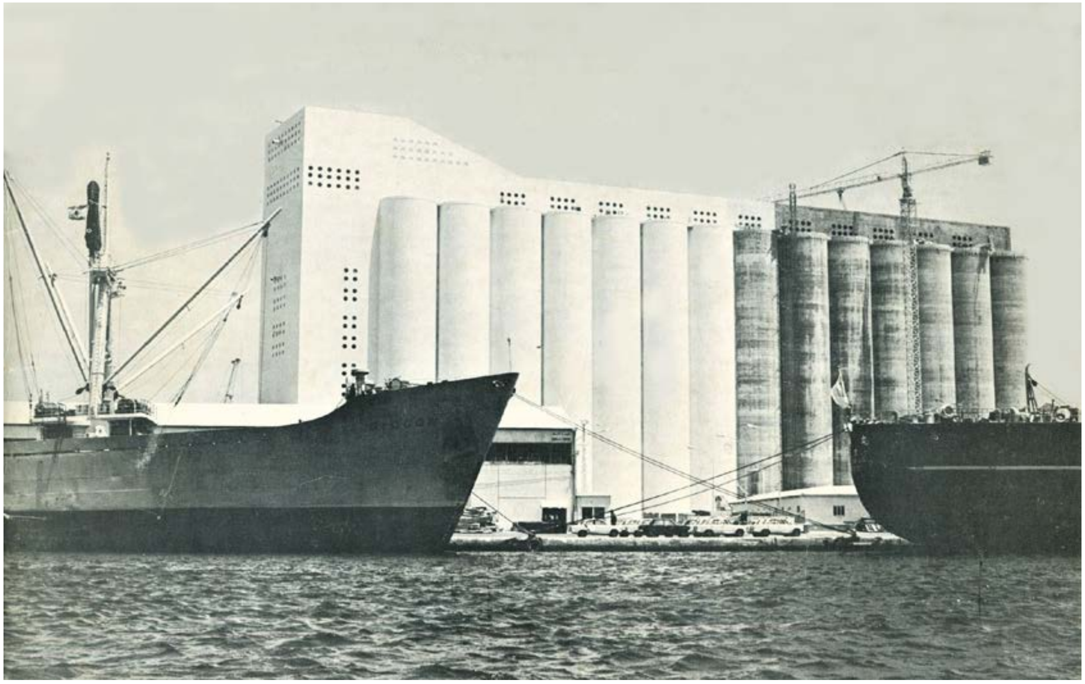

Figure 3: Phase I grain silos completed and Phase II nearing completion (adapted brochure Council for Large Projects-Lebanese Ministry of Public Works, 1970).

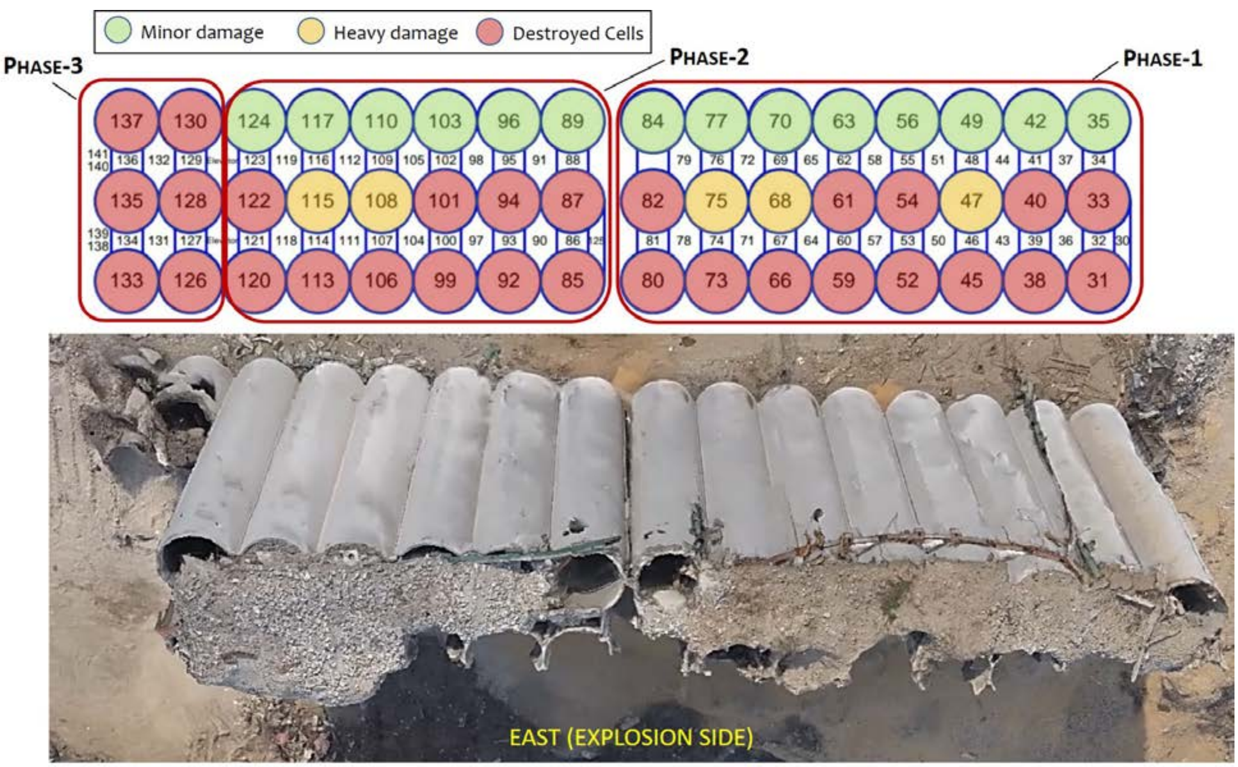

Figure 4: Plan view showing the configuration of the grain silo complex. Color code indicates damage levels from the 4 August 2020 blast. Photo is a composite aerial imagery with laser scan survey looking down (provided by Mr. E. Durand)

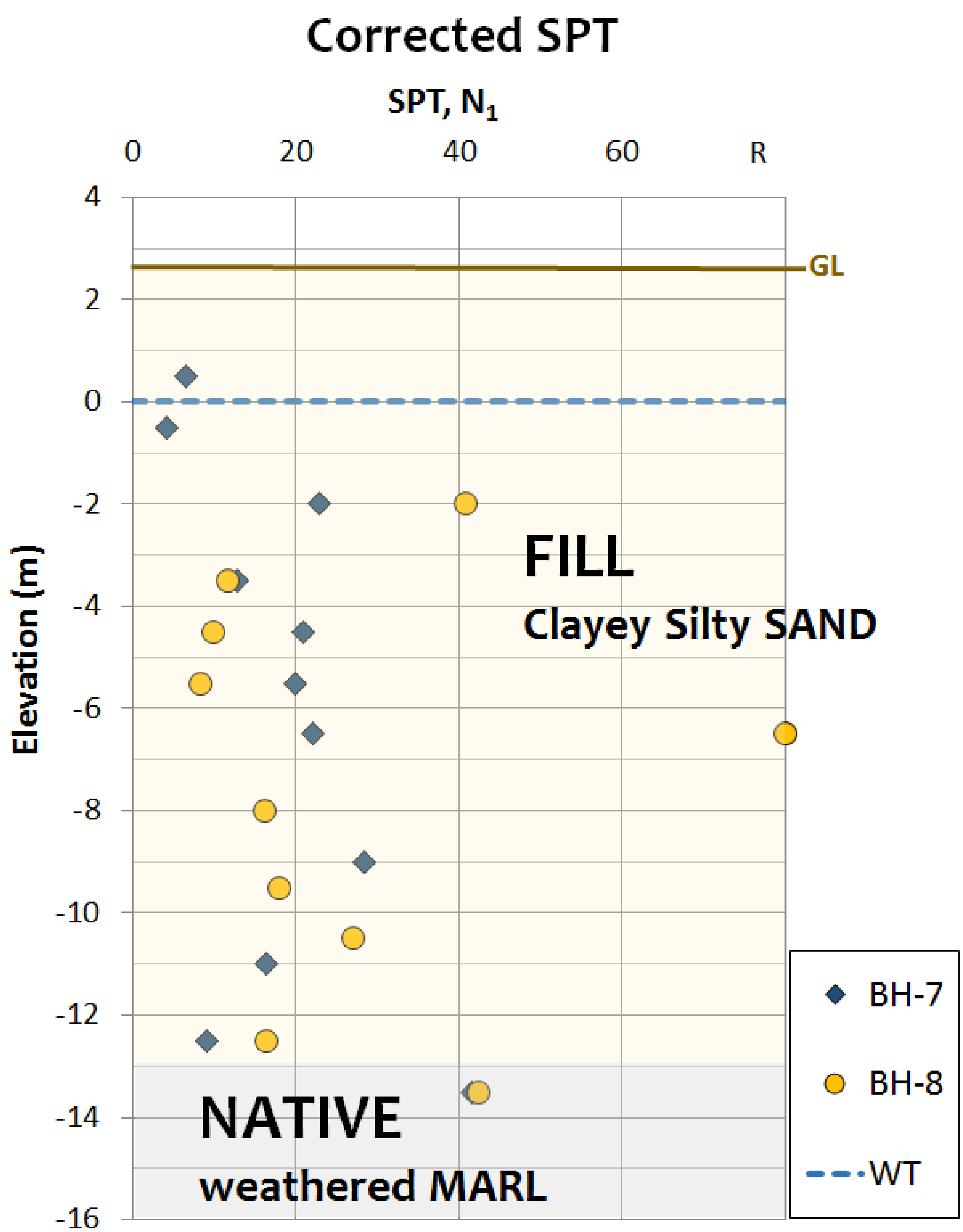

Figure 5: Subsurface profile. The data was taken from boreholes located below the footprint of silos executed in Phase-1 (source-courtesy: *Forex* sarl, geotechnical site exploration co.)

In the late 1990s a structural assessment was conducted on the silos. Significant deterioration of the 17-18 cm thick outer concrete silos shells was observed, mostly due to exposure to the humid and salty seafront environment and subsequent carbonation. The damage was addressed by constructing a 12 cm thick reinforced concrete jacket onto the inner walls of the outer/exposed silos. This strengthening measure improved their response to the blast on 4 August 2020.

Explosion Impacts on Grain Silos

When combined together, the Beirut Port grain silos comprise a substantial structure, roughly 175 m long and 30 m wide, with a height of 50 m. Parts of the silos were full or partially full with grain at the time of the event, thus increasing their mass and the bulk resistance of the thin concrete shell cylinders.

Figure 6 shows the extensive damage to the silos from the explosion, which was as close as 50 m to the silos. The silos visible in the photograph are from the 2nd and 3rd rows, because the first (eastern-most) row of silos was completely destroyed by the blast. Near the base of the silos in Figure 6 is spilled grain. The specific condition of each silo after the blast is shown in Figure 4 using three categories: intact, heavily damaged, and destroyed. The explosion exposed the gap at the construction joint between the Phase I and Phase II silos, which is visible in Figure 6. The gap does not appear to have widened as a result of the blast. Most cells were partially filled at the time of the explosion, except for the six southernmost cells (126 to 137 on Figure 4). Along the west-facing third-row of cells, those that were partially filled survived, whereas those that were empty (at the south end) were completely lost.

Figure 6: View from the east of silos following the blast. Picture taken from Quay 10. (33°54'6.35"N; 35°31'16.19"E).

Multi-epoch LiDAR scans of the silos were performed on September 17 2020, November 23, 2020 and March 28 2021 by Mr. Emanuel Durand of Amann Engineering. These scans allow for the tilt of the surviving silos to be assessed at the times of the scans. Figure 7 shows orthometric views of the west side of the silos from the September 17 scan, with coloration indicating horizontal displacements relative to vertical. The results from this initial scan show a consistent tilt westwards (away from the blast) on the order of 25 cm. Scans taken on November 23 do not indicate any additional movement. As shown in Figure 8, in the time period between November and the last scan taken on March 27, 2021 movements now towards the east have occurred, mainly involving silos that are part of the Northern block (Silos 35 to 82 on Figure 4).

Representative deviations from vertical for Silos 49 and 77 are shown on Figure 9. The reasons for the reversal/recovery of the tilt may be attributed to heavy rainfall causing further erosion and expansion of the crater at the blast epicenter, combined with gradual creep effects at the foundation level now that the piles supporting the silos and/or connecting caps have likely been sheared and/or damaged.

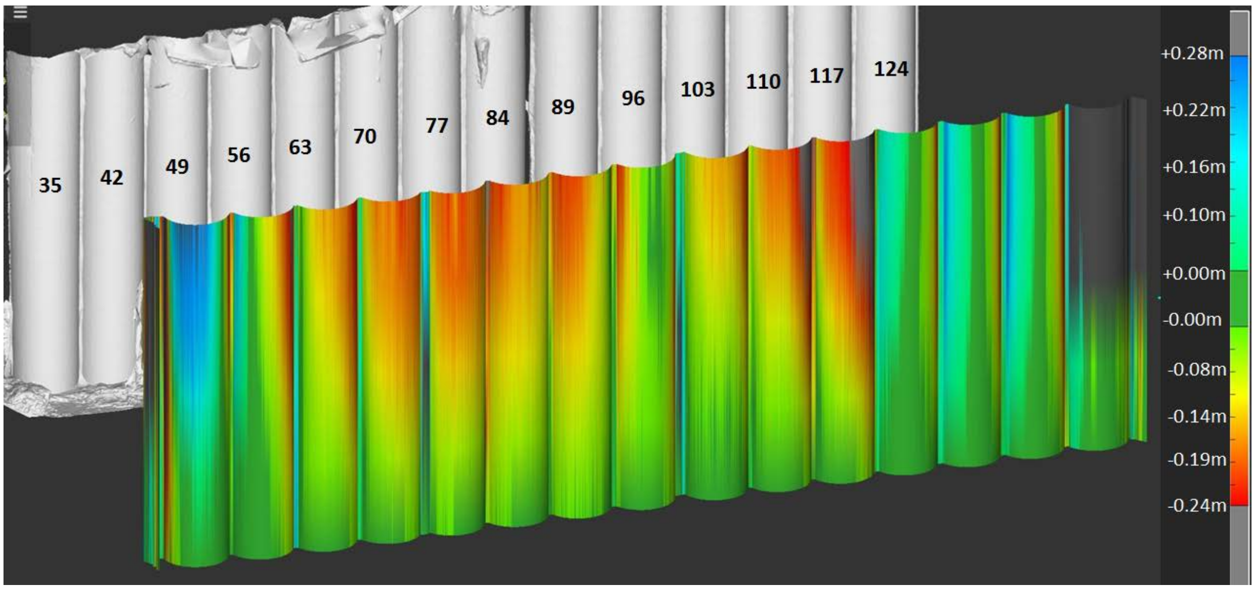

Figure 7: Horizontal deflections of west side of silos as evaluated from LIDAR point cloud data. The horizontal deflections indicate a consistent tilt away from the blast at the top of multiple silos with a maximum of around 24 cm on September 17, 2020 (negative values indicate movement towards the west-away from the blast epicenter). *Adapted from scans provided by Mr. Emmanuel Durand-Amann Engineering.*

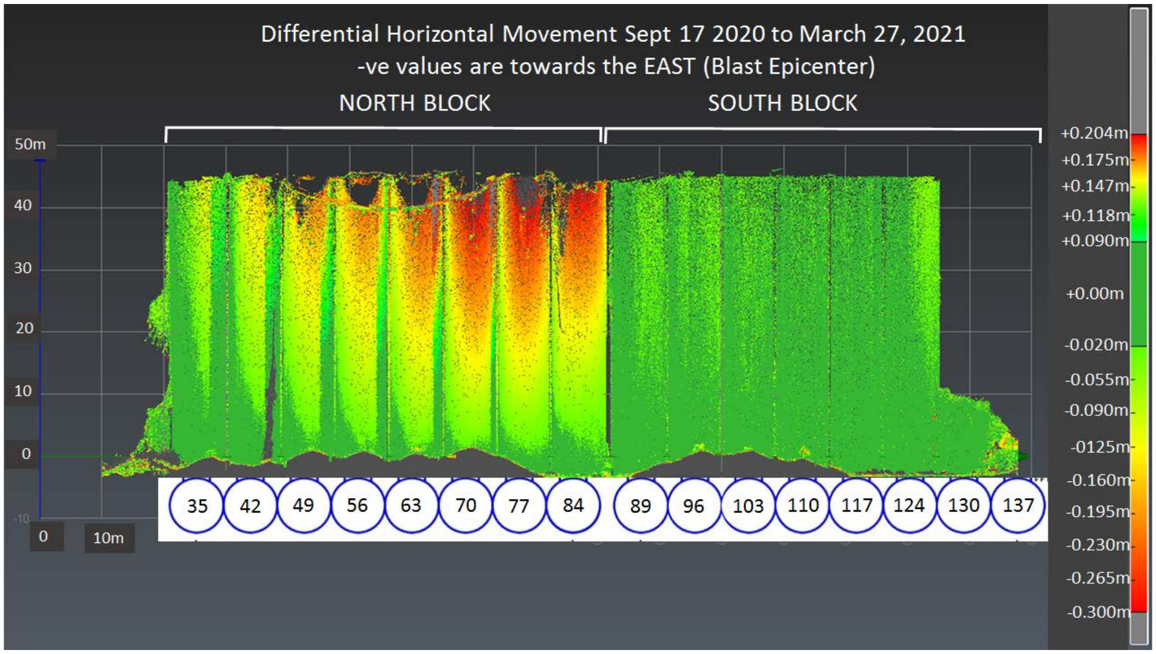

Figure 8: Point cloud data shaded with reference to differential horizontal movement between the date of September 17, 2020-first post blast readings and March 27, 2021 (negative values indicate movement towards the East-towards the blast epicenter). *Adapted from scans provided by Mr. Emmanuel Durand-Amann Engineering.*

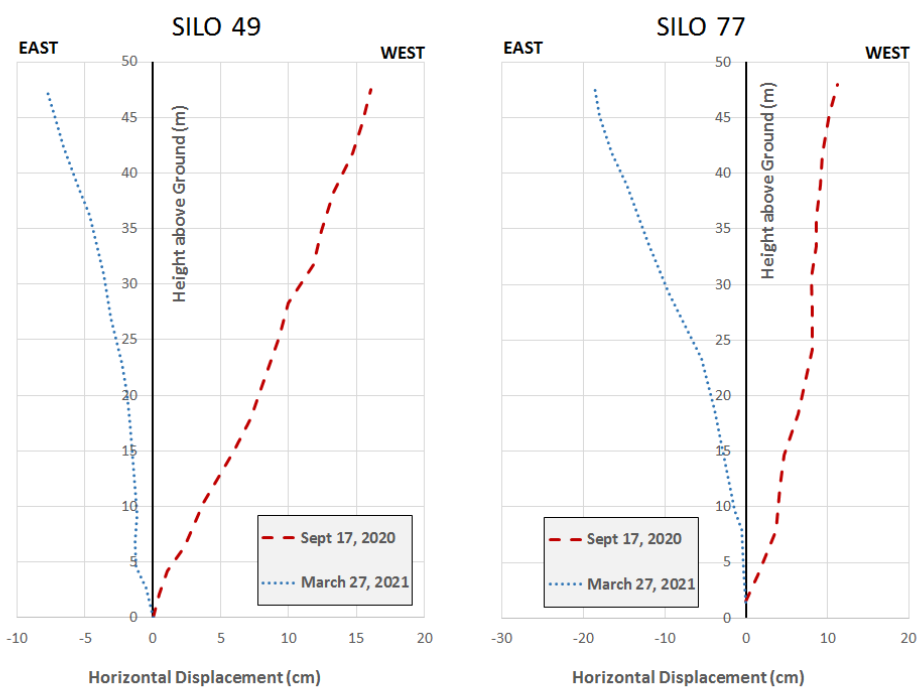

Figure 9 - Representative horizontal movements shown for Silos 49 and 77 (Northern Block) showing the post blast readings (September 17, 2020) and readings taken on March 27, 2021. *Extracted from scans provided by Mr. Emmanuel Durand-Amann Engineering.*

Crater and Quay Wall 9 Flow Slide

The blast at Hangar 12 left a crater of nearly 120 m diameter. Figure 10 includes before and after aerial views of Hangar 12 and the crater. In the aftermath of the event, detailed bathymetric surveys were conducted by teams from the Lebanese army using boat-mounted bottom profilers. This survey provides water depths to ~1cm resolution. The nominal pre-explosion depth in Basin 3 was 10.5 m (this depth was maintained to accommodate the needs of cargo ships serviced by the Port). Figure 11a shows the post-event depth contours 4 days following the blast, and Figure 11b shows a west-east cross-section through the crater.

Figure 10: Aerial views of ground zero (Hangar 12) prior to (31 July 2020) and immediately following (4 August 2020) the explosion (Google Earth).

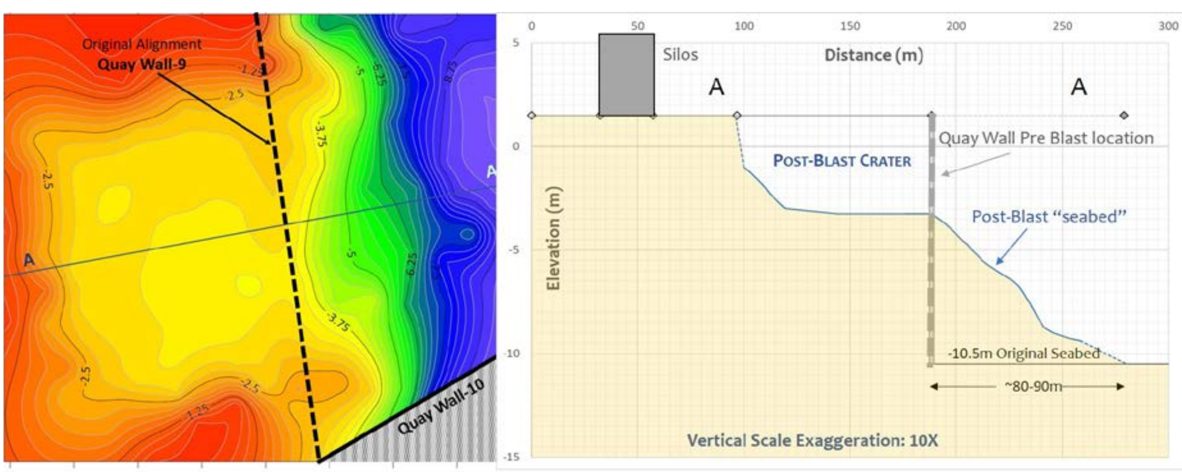

Figure 11: (a) Water depths from bathymetric survey conducted on August 8, 2020; (b) west-east cross-section through center of crater. Bathymetric data from the Lebanese army.

The geometry and size of the crater clearly correspond to the blast location (Hangar 12). The crater is 120 m in diameter and roughly 4.5 to 5 m deep; the depth would likely have been greater had it not been for the presence of water at ~elev. 0m. Volume calculations were conducted on the 3D crater and "flow-out" material into the basin (Sadek et al., 2021a). These showed that the volume of material displaced into the basin was roughly 38,500 m^3, compared to 45,500 m^3 of material lost from behind the original location of the quay wall. The "missing" balance of ~7000 m^3 was likely fill material behind the quay wall and above the water level that was ejected into the air and deposited away from the blast zone. These numbers confirm the likelihood that the material retained by the quay wall flowed/ran out into the basin for a considerable distance as shown in Figure 11b (on the order of 80 m).

Building Impacts

Beirut has a rich architectural history and contains buildings spanning many construction eras. Structures built before the 1950s-60s typically consist of low-rise stone masonry bearing wall buildings developed without adherence to modern building codes. Several of these structures that have architectural or historical value are classified as *heritage* buildings by the Ministry of Culture's Directorate General of Antiquities (DGA). Mid-rise reinforced concrete frame structures emerged in the 1950s. Then, during the Lebanese civil war (1975-1990), building construction was affected by poor building code design provisions and lack of material quality control (Salameh et al. 2016). Despite Lebanon being seismically active, during that era most of the buildings in Beirut were designed to resist gravity loads only, with little or no consideration to lateral resistance. Seismic provisions in building codes were introduced in the 1990's, and although not strictly enforced until 2013 (with the publication of the second edition of the

Lebanese earthquake standards; Libnor, 2013), structures built after 1990 can generally be considered as modern structures. Table 1 summarizes the evolution of the building stock in Beirut with time, namely, the typical structural systems, the design and construction quality, and the building heights.

Table 1: Characteristics of the Beirut building stock (adapted from Salameh et al. 2016).

Year	Structural System	Likely Design and Construction Quality[2]	Height[3]
Before 1935	stone masonry bearing walls[1]	GLD - Good	Low-rise
1935-1955	stone masonry bearing walls[1]	GLD - Good	Low-rise
	mixed stone masonry bearing walls and reinforced concrete frame	GLD - Good	Low-rise; Mid-rise
1955-1975	reinforced concrete frames	GLD - Good	Mid-rise
1975-1990	reinforced concrete frames	GLD - Poor	Mid-rise
1990-2005	reinforced concrete frames and walls	GLD or SD - Good	Mid-rise; High-rise
After 2005	reinforced concrete frames and walls	SD - Good	Mid-rise; High-rise

[1] Slabs are either wooden, reinforced concrete, or steel
[2] GLD = gravity-load design; SD = seismic design
[3] Low Rise: up to 6 stories; Mid Rise: 6 to 12 stories; High Rise: greater than 12 stories

This section describes the GEER team data collection procedures and results. Data collection consisted of in-person building inspections conducted shortly after the blast and street-view imagery about two months after the blast. The reconnaissance approach was strongly affected by the global COVID-19 pandemic, which greatly curtailed international travel, as well as by US-

Lebanon shipping restrictions, which limited our ability to import reconnaissance equipment (e.g., from the NSF-sponsored RAPID site) to assist in the work.

In-Person Building Inspections

The AUB Maroun Semaan Faculty of Engineering and Architecture (AUB-MSFEA) set up an emergency hotline and engineering dispatch center for Beirut residents and businesses concerned about the structural safety of buildings following the Beirut Port explosion. Teams of engineers visually assessed buildings, provided advice on imminent dangers from structural, non-structural, or falling hazards, and recommended possible mitigation measures.

Inspections included visual assessments of the exterior and (in most cases) interior of buildings. The team photographed building façade(s) and structural and/or non-structural damage visible inside or outside of buildings. They completed an assessment survey form for each structure visited. The assessment form was based on the ATC-20 (1995) and ATC-45 (2004) rapid and detailed evaluation safety assessment forms, with modifications to suit the local setting as detailed in Sadek et al. (2021a). An important distinction between these building inspections and those by OEA is that the documentation more specifically delineated damage to structural (i.e., load-bearing) vs non-structural elements, which conforms with protocols widely used in post-earthquake reconnaissance. Some of the damage recorded in these surveys may have preceded the explosion (e.g., shrapnel during the Lebanese civil war, prior settlement of foundations, corrosion due to water leakage), but were still reported in the survey forms. They were distinguished from damage due to the explosion whenever possible through visual identification or when reported as such by the residents.

Figure 12 shows the locations of 172 buildings inspected during this effort, most of which are located within 2 km of the blast.

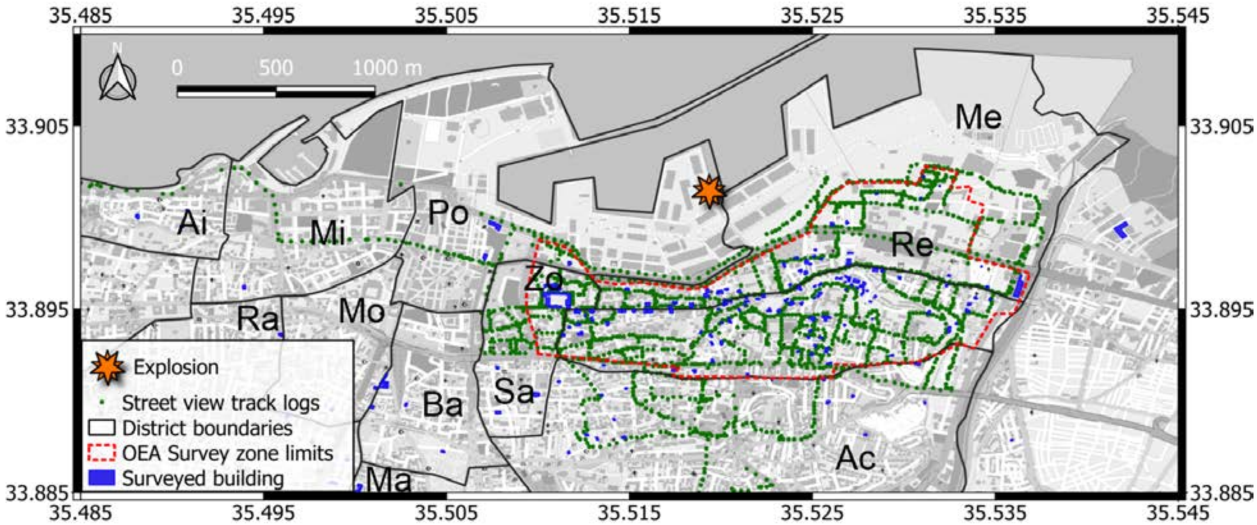

Figure 12. Locations of buildings with in-person inspections and tracks of 360-degree photo surveys from the GEER reconnaissance.

<u>Street-View Photographs</u>

Street-view high-resolution photograph surveys were performed on 8 and 15 October 2020. The purpose of these surveys was to document the damaging effects of the blast for a large number of structures, albeit with less information per structure than the in-person inspections provide.

We originally attempted to utilize street-view equipment owned and maintained by the NSF-sponsored RAPID site, but this was ultimately deemed unworkable. As a result, we instead used a commercially-available GoPro Fusion camera that was mounted to the roof of a car. The camera was used in a mode that allows manual control on the number of images taken in order to ensure an optimal coverage with a practical number of images. All photos were geo-tagged (i.e., the location of the camera is recorded as a latitude/longitude) and the azimuth of the photograph (i.e., the direction that the camera is pointed towards) was recorded. Figure 12 shows the routes taken by the camera-mounted car. Note that this method of reconnaissance could be undertaken safely given the public health challenges that were present at that time in Beirut. All of the images (2100 in total) and the related metadata collected in this survey, were uploaded to mapillary.com and have been archived as described in *Data and Resources*.

Structural Damage Assessment

In this sub-section we describe how the data collected in reconnaissance was interpreted to provide damage classifications, and we present several examples of damage. The interpretation of spatial patterns in the data is presented in a subsequent section.

Structural damage was classified for the buildings with in-person inspections using a system adapted from Bray and Stewart (2000) and EMS98 (Grünthal, 1998). Damage indices range from D0 (no observed damage) to D5 (complete collapse of a floor or the entire structure), as given in Table 2. The index descriptions in Table 2 are specific to this study.

Table 2: Structural damage classifications*. Adapted from Bray & Stewart (2000) & EMS98 (Grünthal, 1998).

Structural Elements	Damage Summary	DAMAGE DESCRIPTORS BY TYPOLOGY	
		SANDSTONE BEARING WALL BUILDINGS	RC BUILDINGS
D0	No Damage		
D1	Light Damage		

Load-bearing structural elements	No damage	Hairline cracks in a few walls Fall of small pieces of plaster only	Fine cracks in plaster over frame elements or in wall bases
Non-structural elements**	Minor damage/cracking		Fine cracks in partition and infill walls
D2	**Moderate Damage**		
Load bearing structural elements	Minor damage / cracks (insignificant displ. across cracks)	Cracks in many walls Fall of large pieces of plaster	Cracks in columns, beams and structural walls.
Non-structural elements	Moderate damage/cracking.	Moderate damage to façade arches or balconies Moderate damage to roof or ceilings	Moderate cracks in partition and infill walls Fall of brittle cladding and plaster. Falling mortar from the joints of wall panels. Moderate to heavy damage of false ceilings.
D3	**Heavy Damage**		
Load bearing structural elements	Significant damage (cracking with significant deformations across the cracks), but no collapse	Large and extensive cracks in most walls Tilting or separation of bearing walls	Cracks in columns and beam column joints of frames at the base and at joints of coupled walls Spalling of concrete cover Buckling of steel rebars
Non-structural elements	Heavy damage/cracking	Failure of individual non-structural elements. Heavy damage or failure of façade arches or balconies Heavy damage to roof or ceilings	Large cracks in partition and infill walls Failure of individual infill panels Heavy damage of false ceilings

D4	Partial Structural Collapse		
Load bearing structural elements	Collapse of a portion of the building.	Serious failure of walls Partial structural failure of roofs and floors	Large cracks in structural elements Compression failure of concrete Fracture of rebars; Bond failure of beam rebars Tilting of columns Collapse of a few columns or a single upper floor
Non-structural elements	Very heavy damage/cracking		
D5	**Full Structural Collapse**		
Complete collapse of a floor or the entire structure			

* Classification is based on the main structure. Any appendages (e.g., an additional room built with masonry blocks on the roof) are not considered in the classification.

** Here, non-structural elements include partition walls, false ceilings, external cladding, balconies, façade arches, and exclude glazing, door and window frames, contents, or equipment.

This classification was applied to the 172 buildings that were inspected in-person by the GEER/AUB-MSFEA team. An additional 10 buildings were classified as having heavy damage (indices D3 to D5) based on the 360° photos described in the previous sub-section. In total, 182 buildings were classified. These buildings consist of 73 Stone Masonry (SM) bearing-wall buildings (for some of these buildings, concrete frames were later added within an existing floor or to build upper levels) and 109 Reinforced Concrete (RC) buildings. These buildings are located at blast distances of 0.6 to 4.4 km, with most being within 2 km.

Figure 13 illustrates RC and SM buildings with variable levels of damage. Figure 13 (a) shows two modern high-rise RC structures with a D2 damage classification. These buildings, located ~700 m from the explosion, sustained moderate damage to non-structural components (e.g., cladding and false ceilings) but no apparent structural damage. Figure 13 (b) shows an SM building that sustained heavy structural damage (D3), namely, significant cracking of its exterior bearing walls, failure of its façade arches and balconies, and partial collapse of its roof. Finally, Figure 13 (c) and (d) show two partially collapsed (D4) and one totally collapsed (D5) SM buildings, respectively. Sadek et al. (2021a) provides additional examples. The damage classification of all 182 buildings is available in the published dataset (Sadek et al., 2021b).

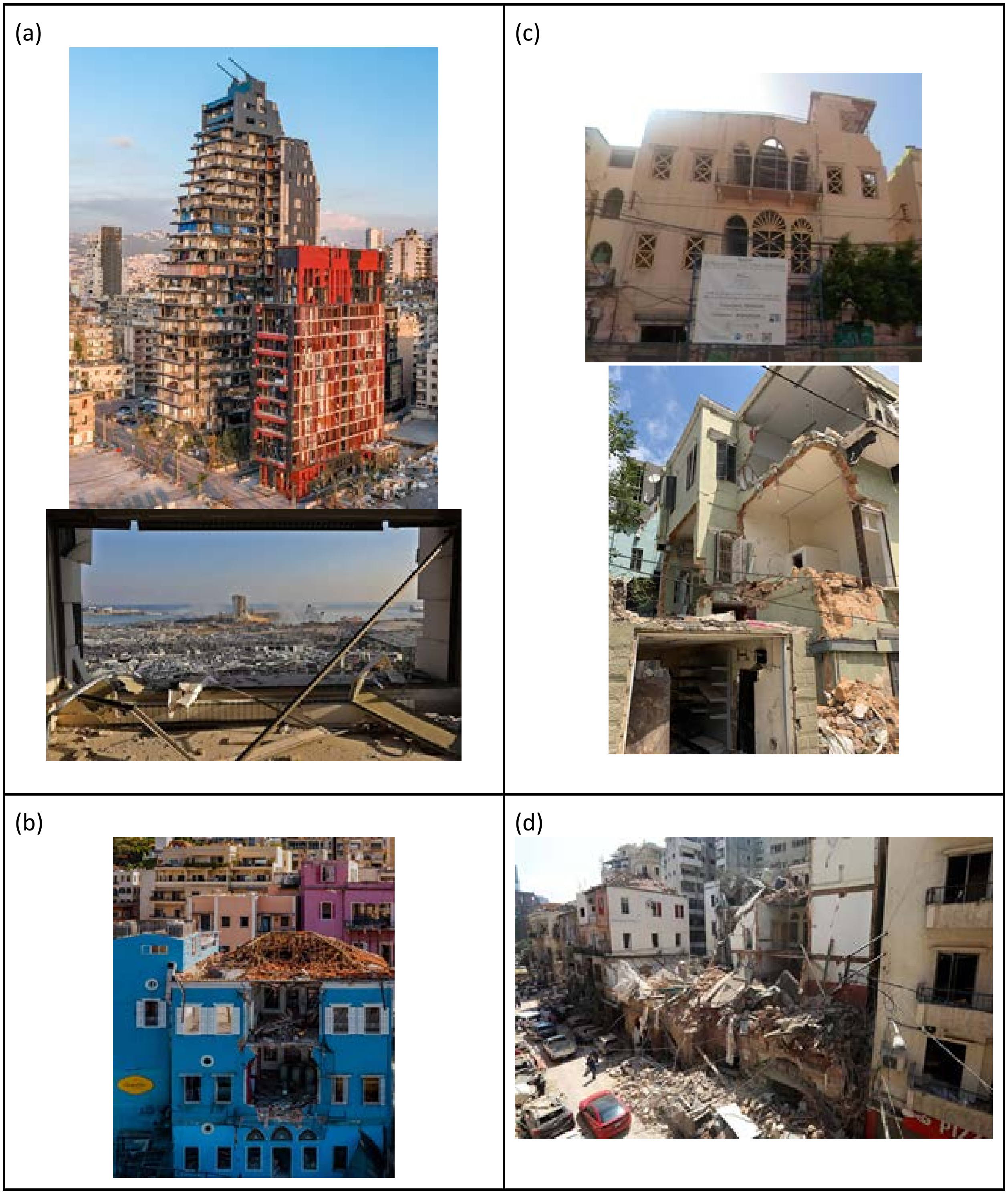
(a)
(c)
(b)
(d)

Figure 13: Examples of buildings with variable levels of damage from the August 4 blast. (a) RC structures that sustained moderate non-structural damage (cladding, false ceilings …) but no apparent structural damage (D2); (b) stone masonry building that sustained heavy damage (D3) with significant cracking of exterior bearing walls, failure of façade arches and balconies, and partial collapse of the roof; (c) partially collapsed stone masonry buildings (D4); and (d) totally collapsed stone masonry building (D5). Sources: (a - upper image) ©RAMI RIZK ; (a - lower image) AP photo by Hassan Ammar; (b) ©RAMI RIZK; © GEER/AUB-MSFEA; and (d) Reuters.

Some of the buildings inspected by OEA (2020) were also assigned a structural damage classification and subsequently used in the analysis of spatial damage patterns. They consist of the buildings reported by OEA (2020) to be partially or totally collapsed and those with partial or total collapse of a roof or slab, and were given a damage classification D4 or D5. The other buildings have not yet received structural damage classifications, because the available information from those inspections does not include photographs and other details needed to support a classification.

Façade Damage Assessment

Using the ~2100 street view photos, we classified façade damage to building openings (windows, doors, and frames). This façade damage assessment was performed remotely by four different investigators. Consistency in the damage assessment process was ensured by cross-checking of results in regular meetings designed to minimize between-investigator discrepancies. The number of inspected façades is greater than the number of analyzed photos as one photo typically contained multiple façades belonging to different buildings. The damage assessment has been performed using QGIS and the results stored in a geodatabase (details in *Data and Resources*). Façade damage was classified according to the damage levels provided in Table 3 (newly developed for this GEER deployment). For each building façade inspected, the geodatabase contains: damage classes, azimuth of the façade, break/blow-out rates (for damage classes 1 and 2), and comments on reconstruction activities taking place in the period between the explosion and dates when the photos were taken.

Table 3: Façade damage to building openings (windows, doors and frames). These classifications are dependent on azimuth *xx*, as defined in the inset.

Façade Impact	**Description**
Wxx-0	No observable effects on windows or doors
Wxx-1-yy	Some windows broken, frames generally intact (yy% break rate). Doors remain in place
Wxx-2-zz	Some window and door/door frames blown out (zz% blow-out rate)
Wxx-3	Nearly complete blow-out of windows, doors, and their frames

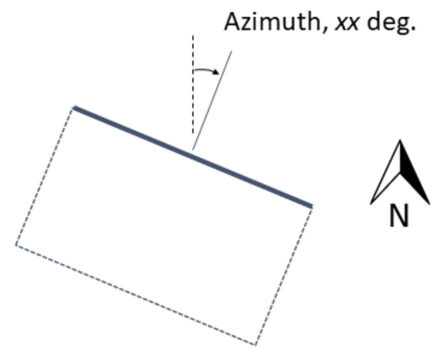

Figure 14 shows example photos of façades experiencing damage classes Wxx-1 where damage was mainly related to broken windows (Figure 14a), Wxx-2 where windows were broken and frames were damaged (Figure 14b), and Wxx-3, the highest façade damage level, where there was complete blow-out of frames (Figure 14c). Photos shown in Figure 14 were taken in different districts of Beirut.

Figure 14. Example of façade damage levels (a) Wxx-1: damage to windows only, (b) Wxx-2: damage to windows and frames, and (c) Wxx-3: complete blow-out of frames.

Damage Pattern Interpretation

Figure 15 shows maps of the spatial distributions of structural and façade damage. The damage is mapped by coloring buildings with classified damage (per Tables 2 or 3). Uncolored buildings are in the AUB-UL database, but lack post-event damage classifications. As shown in Figure 15, the city was also radially divided into three sub-areas, herein denoted the Western, Central and Eastern areas, to examine possible azimuthal differences in the damage distribution.

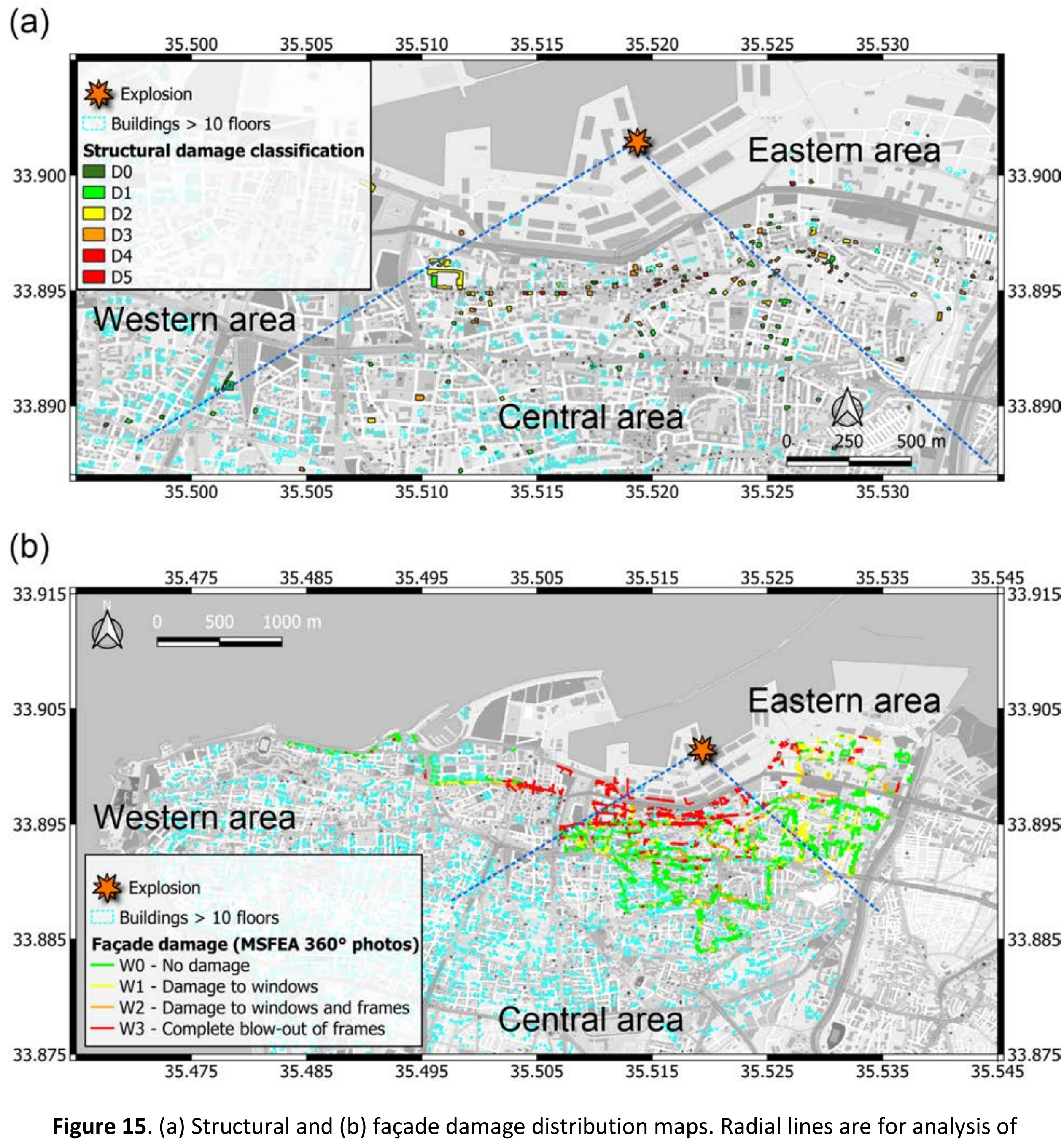

Figure 15. (a) Structural and (b) façade damage distribution maps. Radial lines are for analysis of azimuthal effects on damage patterns.

Because the structural damage data is relatively sparse, damage patterns can be more easily seen in the façade data (Figure 15b). Of the analyzed façades, 5388 of them were classified as Wxx-0, 1158 as Wxx-1, 759 as Wxx-2, and 1920 as Wxx-3. Figure 15b shows that there is a clear fringe area that separates undamaged zones (Wxx-0) from zones with some damage (Wxx > 1). This fringe zone is located at a variable distance from the explosion. It is located at a distance of ~1.5 km from the explosion in the Western area. This distance becomes ~0.7 km-0.9 km in the central area and becomes ~1.2 km in the Eastern area. This analysis suggests that there is a non-symmetric façade damage spatial distribution. It is possible that this pattern is related to the damping effect of tall buildings/structures and/or the different levels of structural vulnerability in different districts of the city.

As described in the introduction of the *Building Impacts* section, Beirut buildings are predominantly of SM and RC construction. The structures most damaged by the blast (D3, D4 and D5) were sandstone bearing-wall structures and older (gravity load designed) RC buildings. Modern RC structures located close to the blast suffered damage mostly to non-structural elements. Figure 16 illustrates the distribution of damage classes D0 to D5 for SM and RC structures based on the in-person survey data only. The data show that the SM buildings generally suffered more damage than RC buildings.

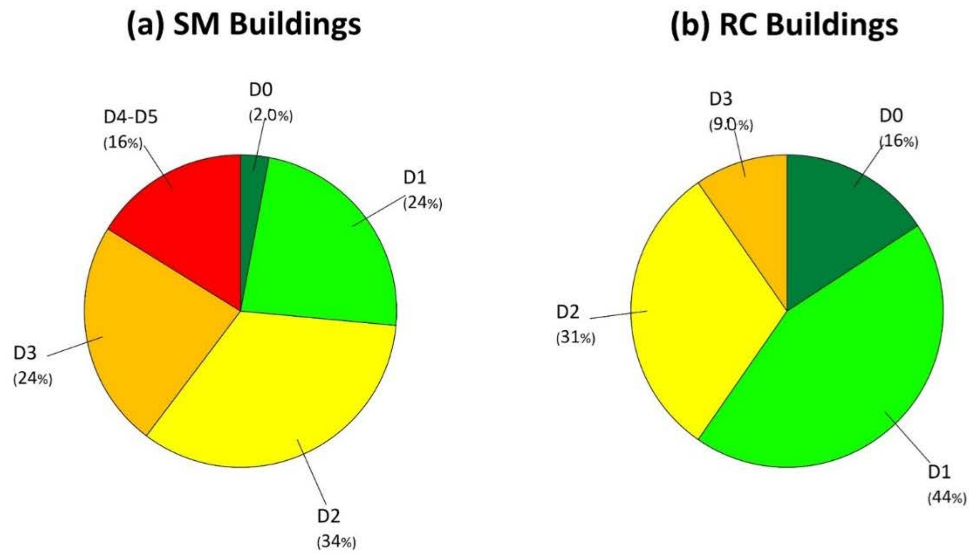

Figure 16. Distribution of damage classes in (a) Stone Masonry (68) and (b) Reinforced Concrete (114) buildings.

Figure 17 shows the distribution of damage classes amongst the assessed structures and facades for the entire city as well as the three sub-areas shown in Figure 15. Figure 17(a) focuses on structural damage, and considers two data populations. The "unbiased" structural sample consists of the 182 structures with in-person and 360° photos inspection (as described in *Structural Damage Assessment*). The second population ("supplemented sample") adds 243 collapsed or partially collapsed buildings (D4-D5) identified by OEA (2020). Those collapsed structures are a subset of those colored in red in Figure 1, after removing "collapses" that involved only balconies and not primary load-bearing systems, based on information in OEA (2020). These additional D4-D5 buildings bias the data set towards higher average damage ratings, in that it does not representatively sample structures across all performance levels. The charts in Figure 17(a) indicate that the most severe structural damage effects are in the central and eastern sub-areas. The apparently severe damage in the eastern sub-area is likely influenced by most of the OEA evaluations having been performed in that part of the city.

Figure 17(b) shows the façade damage distributions. Contrary to the structural damage information, these data indicate that the western sub-area experienced the most relative impact. Because of the much larger sample size in the façade dataset and the aforementioned biased sampling of structural damage, trends in the façade dataset are considered to more accurately represent the spatial distribution of blast impacts in the city. The apparently greater facade damage in the western sub-area of the city may result from a concentration of office buildings in that region, which were slower to be repaired than residential structures that predominate in other sub-areas. It is also possible that directional patterns in damage may be associated with shielding from tall buildings, although such effects can only be speculated upon at the present time and are not discussed further here.

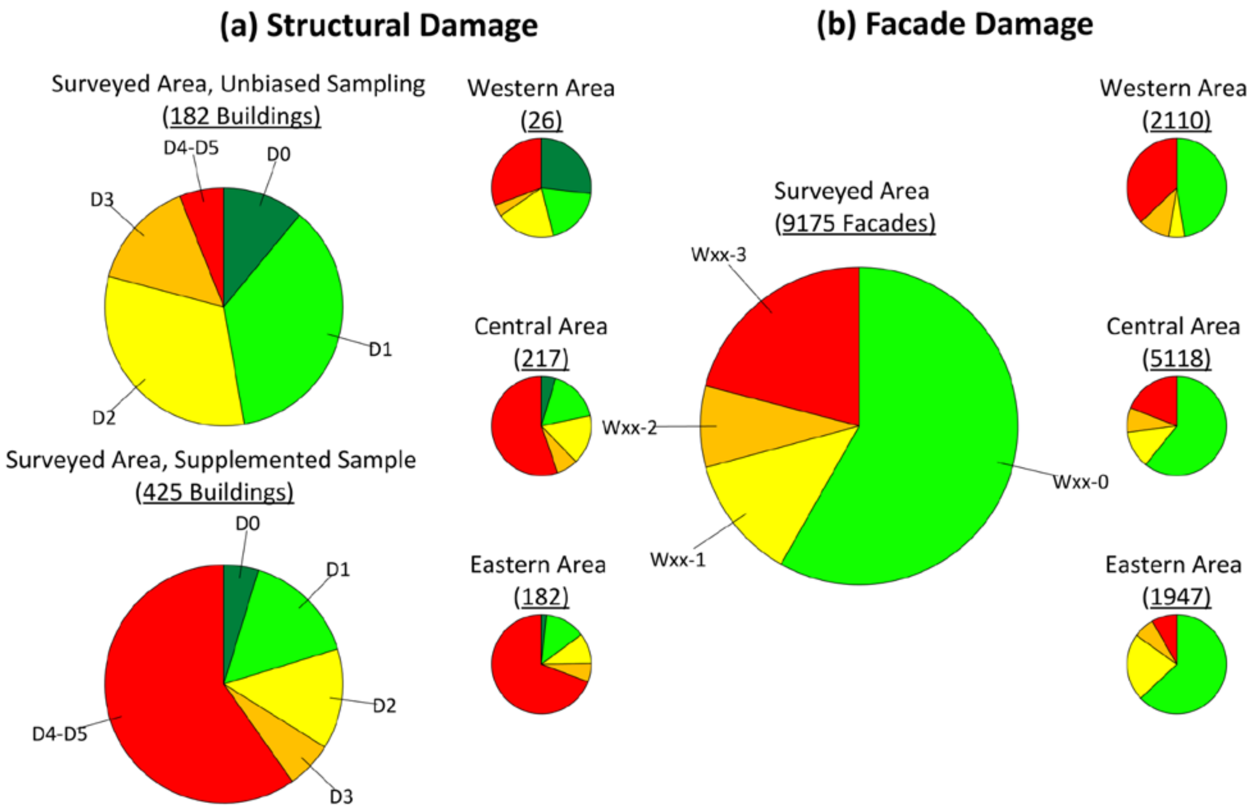

Figure 17 (a) Structural and (b) façade damage distributions by all surveyed areas and sub-areas.

Figure 18 shows variations of damage ratings (represented by box and whisker plots) with distance from the explosion for both the façade and structural datasets. In the box and whisker plots, the two ends of the boxes represent the upper quartile (25% of the data is greater than this value) and lower quartile (25% of the data is smaller than this value), respectively, the line inside the box represents the median value, and two whiskers represent the minimum and maximum values within that category. For both datasets, the most severe damage ratings occur at the closest distances, with less severe damage (on average) occurring at greater distance. These trends were also observed within each of the three sub-areas, although the strength of the distance trend is strongest in the west sub-area. This is likely because most of the structures and façades that were assessed in this area are along the coastline with a direct line-of-sight to the explosion. As a consequence, there are fewer complicating factors (shielding, etc.) that might impede the natural attenuation of damage with distance.

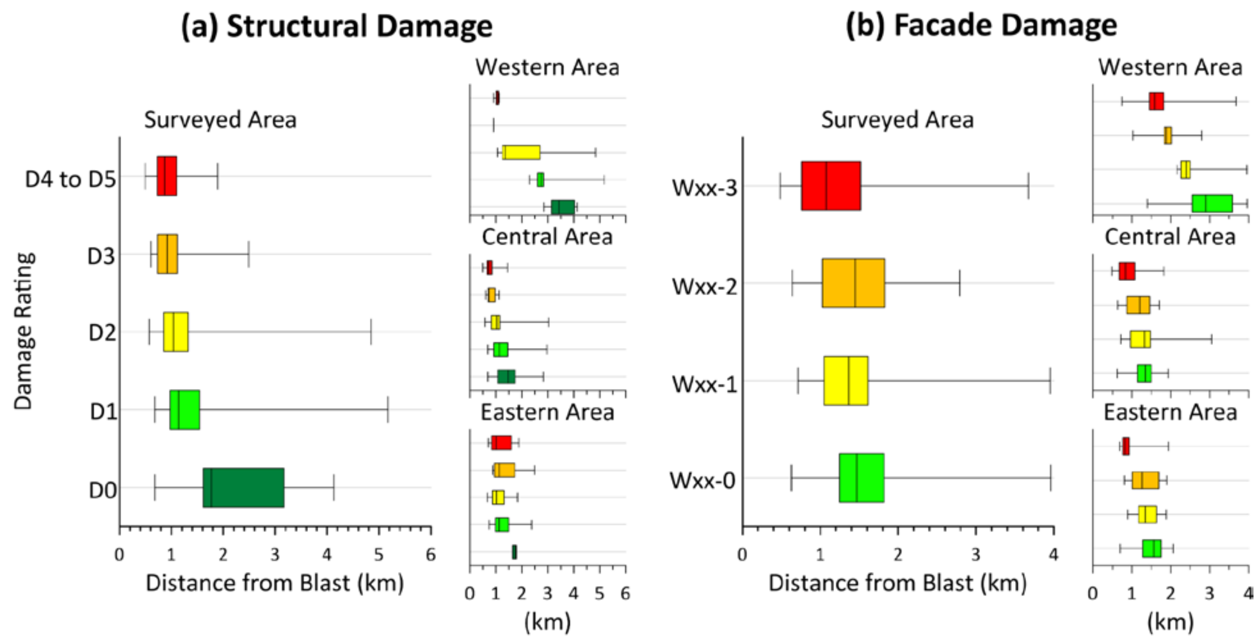

Figure 18 (a) Structural and (b) façade damage variations with distance for all surveyed areas and sub-areas

<u>Comparison to Damage Proxy Maps</u>

Following disasters, the Advanced Rapid Imaging and Analysis (ARIA) team at the Jet Propulsion Laboratory and the Space Geodesy group at the Earth Observatory of Singapore produced Synthetic Aperture Radar (SAR)-based Damage Proxy Maps (DPMs). Such maps are produced using pre- and post-disaster radar data. The technique used to produce DPMs is based on differences in phase statistics of microwaves returning to a satellite (e.g., Fielding et al., 2005; Yun et al., 2011; Yun et al., 2015).

Following the August 4, 2020 Beirut explosion, a DPM was produced using SAR radar data from the Copernicus Sentinel-1 satellites. This DPM was generated by comparing pre- and post-explosion SAR scenes acquired from four different tracks. The satellite tracks view Beirut from the west (two) and the east (two), with look-angles from vertical ranging between 31°-44°. The map used 12 pre-event and two post-event SAR scenes between May 1, 2020 and September 1, 2020. The map covers an area of 13 by 16 km (Figure 19). Each pixel size is about 10 by 10 m. Colored pixels represent zones where there was significant change in radar wave scattering at the reflectors (i.e., ground surface or buildings), which may indicate damage from the stressing event.

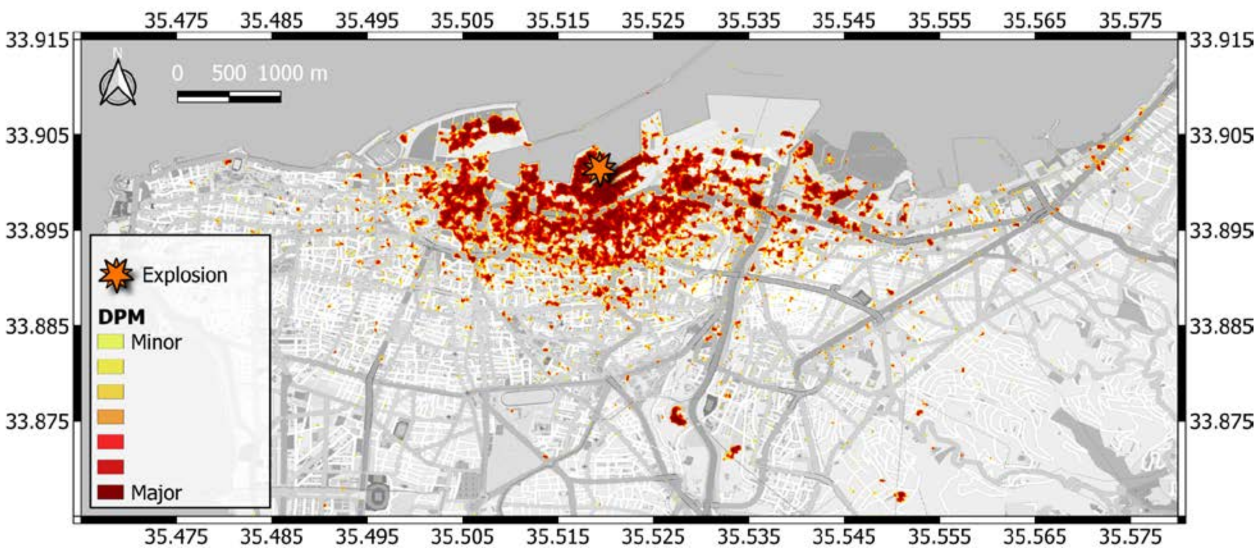

Figure 19: DPM produced following the 4 August, 2020 blast explosion (data source: NASA-JPL)

Figure 20 shows a box and whisker plot highlighting how DPM correlates with structural damage; DPM in this plot has been converted to a numerical index between 0 and 1.0. This index corresponds to the colors on maps over the index range of 0.75-1.0, as shown in the plot (the index range of 0-0.75 produces no map coloration). The undamaged structures consistently occur at index values < 0.75, and the damaged structures occur at index values > 0.75. Among structures with damage (classes D1 to D5), DPM index is highest for structures with full or partial collapse (D4-D5) (median > 0.9) and is approximately the same (median of about 0.8) for structures with lower damage states D1 to D3. This indicates an ability of the DPM index to distinguish among damage levels at a high level (no damage, damage, collapse), but not to distinguish among damage levels short of collapse.

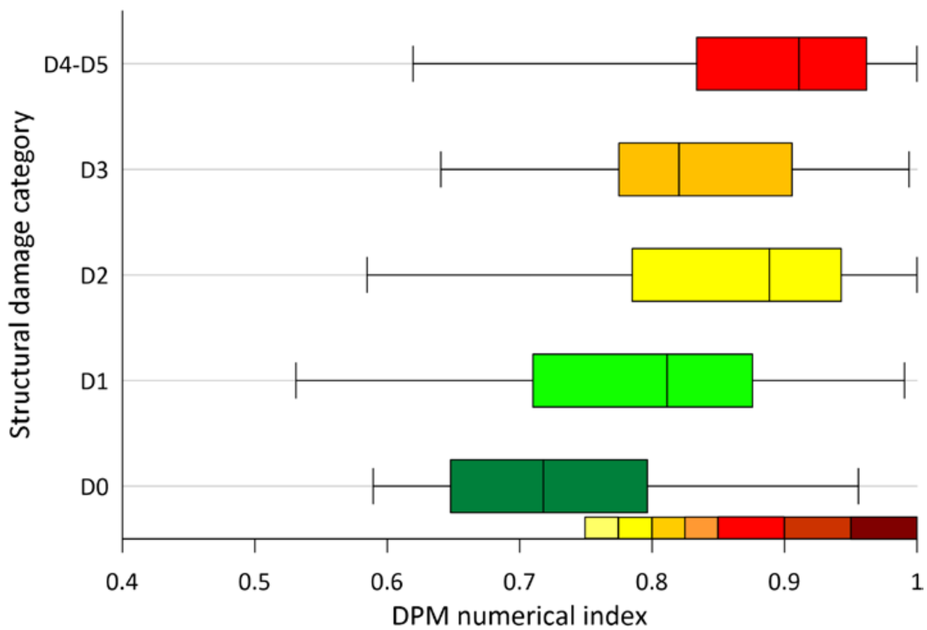

Figure 20: Relationship between numerical index of DPM (0-1) and structural damage categories

Figure 21 shows a box and whisker plot highlighting how DPM correlates with façade damage. The undamaged state (Wxx-0) has a median DPM index near the lower limit of shading (about 0.75). Among structures with façade damage, DPM index cannot distinguish between damage levels Wxx-1 and Wxx-2 (median DPM index of about 0.8), whereas the strongest level of damage (Wxx-3) has a clearly higher median DPM index of 0.9.

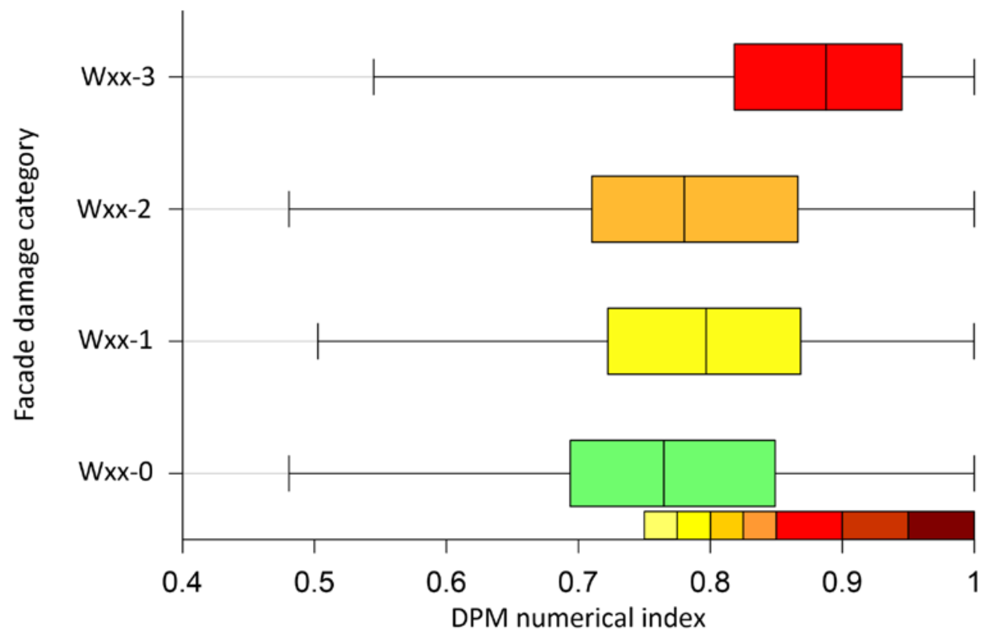

Figure 21: Relationship between numerical index of DPM (0-1) and façade damage categories.

Summary and Conclusions

We present data compiled from reconnaissance of the effects of the 4 August 2020 explosion on Beirut infrastructure. We describe impacts on the Port of Beirut where the explosion occurred and buildings in the city up to a distance of approximately 4 km. This paper is derived from a report by the GEER Association (Sadek et al. 2021a), with some updates where additional information has become available.

For the Port, impacts are documented to Quay Wall 9, which collapsed as part of a flow slide in which a crater formed at the blast site and presumably liquefied fill material flowed into the adjacent Basin 3. We also describe impacts on a series of grain silos located as close as 50 m from the blast source. Most of the silos were lost as a result of blast impact, although a row of silos (furthest from the blast) survived. That row of silos initially tilted towards the west by amounts up to ~0.5%, and in the nine months since the blast, some of those silos experienced a reversal in the direction of tilt to a maximum of ~0.5% towards the east (i.e a net slope reversal of ~1%).

In portions of Beirut west, south, and east of the explosion, different levels of damage occurred to buildings, varying from full collapse to no structural or façade damage at blast distances under 4 km. It is noteworthy that sporadic damage due to the blast extended to much farther distances in the form of broken windows and doors and impacting some facilities at the Beirut Rafic Hariri International Airport 8 km away from the explosion. We document both structural impacts and façade damage (mainly to windows and doors) as derived from structure-specific inspections and interpretation of street view imagery. We show that the attenuation of damage with distance from the source is azimuth-dependent, decaying relatively rapidly in the central and eastern sub-areas of the city (areas of relatively dense urbanization with many buildings) and decaying more gradually to the west (where the blast pressure pulse was able to travel relatively far before encountering buildings).

The data collected from post-event reconnaissance (Sadek et al., 2021b) can be used in future research on a variety of topics, which include:

1. Analysis of the blast impact on the silo structure to see if the observed collapses, and survivals, of particular silos is predictable. The tilt of the silo foundations and its time variation is also of interest.
2. Analysis of the apparent flow slide to derive residual strengths, and pairing this with penetration resistance data for the remaining portions of the Port fill (Figure 5).

3. Based on inspections and imagery from OEA (2020), expand the inventory of buildings with classified structural damage and update the analyses utilizing this data set.
4. The factors affecting damage distributions in Beirut can be studied using dynamic simulations of the blast pulse through the city. Factors such as shielding of some portions of the city from tall intervening structures is a topic of particular interest.
5. Further analysis of DPM effectiveness regarding the damage from the blast and tracking of recovery as buildings are repaired.

Data Availability

Some or all data, models, or code generated or used during the study are available in a repository online in accordance with funder data retention policies. The damage proxy map used in this study was retrieved from the NASA-JPL ARIA event page at https://aria-share.jpl.nasa.gov/20200804-Beirut_Blast/ (last accessed June 2021). Locations of 360° photos taken in October 2020, detailed structural damage assessment information for 172 buildings based on in-person inspection performed within a month from the explosion and exterior structural damage assessment information for 10 buildings based on 360° photos taken in October 2020, and façade damage assessment data based on facade damage observed using the 360° photos taken in October 2020 are available in DesignSafe (Sadek et al., 2021b; https://doi.org/10.1007/s00193-020-00970-z). All 360° photos are available in the Mapillary (https://www.mapillary.com/app/?lat=33.90191008577155&lng=35.49106252100046&z=14.512378027628445) and Beirut recovery websites (https://beirutrecovery.org/). For both websites, photos can be visualized after selecting user: aubmsfea in the main menu.

Acknowledgements

The work of the GEER Association, in general, is based upon work supported in part by the National Science Foundation through the Geotechnical Engineering Program under Grant No. CMMI-1826118. Any opinions, findings, and conclusions or recommendations expressed in this material are those of the authors and do not necessarily reflect the views of the NSF. Any use of trade, firm, or product names is for descriptive purposes only and does not imply endorsement by the U.S. Government. The GEER Association is made possible by the vision and support of the NSF Geotechnical Engineering Program Directors: Dr. Richard Fragaszy and the late Dr. Cliff Astill. GEER members also donate their time, talent, and resources to collect time-sensitive field observations of the effects of extreme events.

Part of the research was sponsored by the NASA Earth Science Disasters Program (Grant Number 18-DISASTER18-0034) and performed in collaboration with Sang-Ho Yun of the Jet Propulsion Laboratory, California Institute of Technology.

Many people contributed to the reconnaissance reported here. They are listed in the Acknowledgements section of GEER (2021). We would like to call special attention to Mr. Emmanuel Durand (Amann Engineering, Switzerland) for generously sharing his time and monitoring data.

References

Al-Hajj, S, AH Mokdad, & A Kazzi (2021). Beirut explosion aftermath: lessons and guidelines. *Emergency Medicine Journal*. doi: 10.1136/emermed-2020-210880

Aouad, C, W Chemissany, P Mazzali, Y Temsah, and A Jahami (2020). Beirut explosion: Energy yield from the fireball time evolution in the first 230 milliseconds. arXiv preprint arXiv:2010.13537.

Applied Technology Council, ATC (1995). *ATC-20-2 Report, Addendum to the ATC-20 Postearthquake Building Safety Evaluation Procedures.*

Applied Technology Council, ATC (2004). *ATC-45 Field Manual: Safety Evaluation of Buildings after Windstorms and Floods.*

Beirut Order of Engineers and Architects, OEA (2020). *Beirut Port Explosion of Aug 04 2020: Buildings Final Structural Assessment Report*. OEA. Date: 12 Aug-17 September 2020.

Bray, JD, JP Stewart (2000). Chapter 8: Damage patterns and foundation performance in Adapazari. Kocaeli, Turkey Earthquake of August 17, 1999 Reconnaissance Report, TL Youd, JP Bardet, and JD Bray, eds., *Earthquake Spectra*, Supplement A to Vol. 16, 163-189.

Dechy, N, T Bourdeaux, N Ayrault, M-A Kordek and JC LeCoze (2001). First lessons of the Toulouse Ammoonium Nitrate disaster, 21st September 2001, AZF Plant France, *J. of Hazardous Materials,* 111, 131-138

Diaz, JS (2020). Explosion analysis from images: Trinity and Beirut, Physics Education, https://arxiv.org/abs/2009.05674

Fielding, EJ, M Talebian, PA Rosen, H Nazari, A Jackson, M Ghorashi, and R Walker (2005). Surface ruptures and building damage of the 2003 Bam, Iran, earthquake mapped by satellite Synthetic Aperture Radar interferometric correlation, *J. Geophys. Res.* 110, no. B03302.

Grünthal, G (1998). European macroseismic scale 1998. European Seismological Commission (ESC).

Ismail, S, W Raphael, and E Durand (2021). Case study of the Beirut port explosion using 3D laser scan and non-linear finite element model. *Research on Engineering and Materials*, http://dx.doi.org/10.17515/resm2021.286st0428.

Lebanese Red Cross LRC (2020). Disaster Management Sector Beirut Port Explosion Response Assessment Results (MSNA, DANA) as of August 24, 2020. https://reliefweb.int/sites/reliefweb.int/files/resources/dm-rp-msna-dana-200825.pdf.

Nemer, TS (2021). The Beirut port explosion: A geoscience perspective, Seismological Research Letters. doi:10.1785/0220210051.

Order of Engineers and Architects OEA, (2020). Beirut explosion: Buildings' weekly structural assessment report. https://www.oea.org.lb/Library/Files/news/2020/sep%202020/building%20Weekly%20Report%203.pdf?fbclid=IwAR0fH4X7Ksp0GdbQMHDypWPmgTY25FFX2RFruy5rJmOyjR3KVWLBIOahT-VU

Pilger, C, P Hupe, P Gaebler, A Kalia, F Schneider, A Steinberg, ... and L Ceranna (2020). Yield estimation of the 2020 Beirut explosion using open access waveform and remote sensing data. https://eartharxiv.org/repository/object/1930/download/4053/

Rathje, EM, C Dawson, JE Padgett, J-P Pinelli, D Stanzione, A Adair, P Arduino, SJ Brandenberg, T Cockerill, M Esteva, et al. (2017). DesignSafe: A new cyberinfrastructure for natural hazards engineering, *Nat. Hazards Rev.* 18, 06017001.

Rigby, SE, TJ Lodge, S Alotaibi, AD Barr, SD Clarke, GS Langdon, A Tyas (2020). Preliminary yield estimation of the 2020 Beirut explosion using video footage from social media. *Shock Waves*, https://doi.org/10.1007/s00193-020-00970-z

Sadek, S, M Dabaghi, I Elhajj, P Zimmaro, YMA Hashash, S-H Yun, TM O'Donnell, JP Stewart (2021a). Engineering impacts of the August 4, 2020 Port of Beirut, Lebanon explosion, *GEER Report 070*, Geotechnical Extreme Event Reconnaissance Association, https://doi.org/10.18118/G6C96C.

Sadek S, M Dabaghi, P Zimmaro, YMA Hashash, T O'Donnell, JP Stewart (2021b). In person damage assessment and 360° photo collection and analysis, in GEER - August 4, 2020 Beirut Port Explosion. DesignSafe-CI. DOI: 10.17603/ds2-rh78-ak38.

Search and Rescue Assistance in Disasters (SARAID - www.saraid.org) (2021). Post-Deployment Report: Beirut Explosion 6th - 12th August, 2021. Source: available via the Virtual on-Site and Coordination Centre (VOSOCC) https://vosocc.unocha.org

Temsah Y, A Jahami and C Aouad (2021). Silos structural response to blast loading. *Engineering Structures*, **243**, 22p. https://www.sciencedirect.com/science/article/pii/S014102962100821X

Valsamos, G, M Larcher, and F Casadei (2021). Beirut explosion 2020: a case study for a large-scale urban blast simulation. *Safety science*, **137**, 105190.

World Bank Group (2020). Beirut Rapid Damage and Needs Assessment, August 2020

Yu, GD, Y Wang, L Zheng, J Huang, JL Li, LZ Gong, ... and YS Duh. (2021). Comprehensive study on the catastrophic explosion of ammonium nitrate stored in the warehouse of Beirut port. *Process Safety and Environmental Protection*, **152**, 201-219.

Yun, S, EJ Fielding, M Simons, P Rosen, S Owen, and F Webb (2011). Damage proxy map of February 2011 M 6.3 Christchurch earthquake using InSAR coherence, 8th International Workshop on Advances in the Science and Applications of SAR Interferometry, Frascati, Italy, 19–23 September 2011, link. (last accessed Nov 2020).

Yun, S, K Hudnut, S Owen, F Webb, M Simons, P Sacco, E Gurrola, G Manipon, C Liang, EJ Fielding, et al. (2015). Rapid damage mapping for the 2015 Mw 7.8 Gorkha earthquake using Synthetic Aperture Radar data from COSMO–SkyMed and ALOS-2 Satellites, *Seismol. Res. Lett.* **86**, 1549–1556.

Zhang, X, Y Ding, & Y Shi (2021). Numerical simulation of far-field blast loads arising from large TNT equivalent explosives. *Journal of Loss Prevention in the Process Industries*, **70**, 104432.